Physically-based Neural BRDF

*Alejandro Sztrajman[1], *Chenliang Zhou[1], Gilles Rainer[2], Fangcheng Zhong[1], Cengiz Oztireli[1], and Rafal Mantiuk[1]

[1] University of Cambridge, United Kingdom
[2] Imperial College London, United Kingdom

Abstract. We introduce a novel continuous representation for material appearance based on neural fields. Our model performs accurate reconstruction of real-world materials, while uniquely enforcing all the requisite physical properties for realistic Bidirectional Reflectance Distribution Function (BRDF) data. We conduct a systematic analysis of the enforcement of Helmholtz reciprocity and energy conservation, highlighting the benefits of following physical laws in the visual quality of reconstructed materials. Furthermore, we improve the colour accuracy of Neural BRDFs by supervising not only the individual RGB channels but also the norm of the prediction. We demonstrate on databases of measured real-world BRDFs that Neural Networks that follow these physical constraints represent the original data more faithfully and are much more stable to render with.

Keywords: Neural Fields · Material Appearance · Physics-based Modelling

1 Introduction

Representational learning has become the standard method to model complicated spatial distributions and functions from measured data in Computer Graphics and Vision. Applications of the overfitting of a small neural network to a measured instance of a problem range from 2D images [29] to directional reflectance functions [27, 30] to scene density and radiance [20, 26], and have demonstrated superior expressiveness, interpolation ability and fidelity to the driving data, over analytic parametric models. However, this expressiveness also entails a lack of constraints of the function learnt by the network, which is often addressed through the use of priors (e.g. minimizing total variation) or inductive biases about the problem at hand – e.g. NeUS [32] is premised on the convergence of the reconstructed geometry to a surface.

In the domain of material appearance modelling, the functions used for rendering such as the *Bidirectional Distribution Reflectance Function* (BRDF) [23] have been derived through first principles and obey strict physical constraints. Helmholtz reciprocity ensures that reflected and absorbed energy are agnostic to the direction of light travel, while energy conservation ensures that a point cannot reflect more light than it receives. Parametric BRDF models [11] respect these constraints by design, whereas black-box models such as *Multi-Layer*

Perceptrons (MLP), while optimised to match measured data as accurately as possible, are not guaranteed to comply.

In this paper, we investigate a method to ensure Neural BRDFs respect physical and perceptual constraints, and the impact of this on the learnt result. The contributions of this work are the following:

- a neural BRDF parameterization that guarantees Helmholtz Reciprocity
- a training loss that incorporates and ensures energy conservation of the converged model
- a training loss to avoid chromatic inaccuracies

We demonstrate through systematic evaluation that each of these physically-based constraints contributes to numerically and perceptually more accurate neural BRDFs, highlighting the need for physically-based neural networks to bridge the gap between well-established models like BRDFs and real-world data.

2 Related Work

Replicating the appearance of real-world materials has been a very prolific research fields in Compute Graphics. In this section, we review the most relevant works on acquiring, representing and fitting real-world BRDFs via measurements.

2.1 Material Acquisition and Databases

Traditionally, material reflectance has been measured with Gonioreflectometers, devices that can control the light and view direction and measure the reflected radiance [16, 35]. Various setups exist, some using specific geometries or configurations to measure numerous values at once [2, 18], going as far as measuring entire material patches [5, 34]. These scanners have led to the construction of well-known BRDF databases [7, 19, 24], which we will rely on in this work.

2.2 BRDF modelling

Analytic models have been the most common representations for Bidirectional Reflectance Distribution Functions (BRDFs). They are characterised by their ease of editing, fast evaluation speeds and minimal memory requirements. Classic models include Phong [25], Cook-Torrance [4], Ward [33], Lafortune [14], GGX [31] and Disney [3]. Despite their multiple advantages, their reliance on simplified assumptions about the distributions of reflectance results in a limited ability to accurately reconstruct real-world materials [10, 21].

Data-driven representations offer a powerful alternative by directly leveraging real-world measurement data. A common approach involves the use of tabular data [19], sampling reflectance at discrete intervals of directions and wavelengths. This allows for high-fidelity material reconstruction but suffers from high dimensionality, leading to significant challenges in terms of storage and ease of editing. Dimensionality reduction techniques [15, 19, 24] can mitigate these issues, but they do so at the cost of a reduced reconstruction accuracy.

Neural BRDFs. Neural networks present a modern data-driven alternative, employing neural networks to learn a dense, continuous representation of BRDF data [30]. These models excel in accuracy and efficiency, providing a scalable solution for a broad spectrum of materials while maintaining a compact memory size. However, a notable limitation of neural representations is their lack of enforcement of two fundamental BRDF physical constraints: energy conservation and Helmholtz reciprocity. This oversight can lead to physically implausible results, underscoring the need for additional mechanisms to ensure physical validity and realism.

Many different variants of neural reflectance models have been proposed: Sztrajman et al. [30] introduced the *Neural BRDF* (NBRDF), where a single MLP is overfitted to a given material by training with the measured BRDF. Zheng et al. [38] concurrently proposed a similar continuous representation, while Hu et al. [13] output a tabulated BRDF again. Fan et al. [8] use a universal decoder, for layered BRDFs, such that their BRDF descriptors all exist in the same latent space and Guo et al. [12] learn the mapping from parameters of explicit BRDF models into this neural domain. In order to speed up the conversion of real-world BRDFs into models, Fischer et al. [9] and Liu et al. [17] propose methods to accelerate the fitting as well as optimize the sampling pattern. Other efforts have been made towards real-time rendering with neural BRDFs, by investigating the parametrization [6] or the hardware integration [36].

3 Background

When a beam of light reaches the surface of a material, the intensity is scattered with a distribution determined by the complex interaction between material and light. This is expressed by the Bidirectional Reflectance Distribution Function (BRDF) as described by Nicodemus *et al.* [22], which quantifies the ratio between the reflected differential radiance L_o and the incoming differential irradiance E_i, in the point of incidence:

$$f_r(\theta_i, \phi_i, \theta_o, \phi_o) = f_r(\boldsymbol{\omega}_i, \boldsymbol{\omega}_o) = \frac{\mathrm{d}L_o(\boldsymbol{\omega}_o)}{\mathrm{d}E_i(\boldsymbol{\omega}_i)}\,. \tag{1}$$

This function depends on the incidence angles θ_i, ϕ_i and the outgoing angles θ_o, ϕ_o. For physical plausibility, BRDF functions need to adhere to three fundamental properties:

- Non-negativity: For any pair of directions $\boldsymbol{\omega}_i, \boldsymbol{\omega}_o$: $f_r(\boldsymbol{\omega}_i, \boldsymbol{\omega}_o) \geq 0$;
- Helmholtz reciprocity: For any $\boldsymbol{\omega}_i, \boldsymbol{\omega}_o$, $f_r(\boldsymbol{\omega}_i, \boldsymbol{\omega}_o) = f_r(\boldsymbol{\omega}_o, \boldsymbol{\omega}_i)$.
- Energy conservation: Reflected energy cannot exceed incident energy; *i.e.*,

$$\int_\Omega f_r(\boldsymbol{\omega}_i, \boldsymbol{\omega}_o) \cos\theta_o \mathrm{d}\boldsymbol{\omega}_o \leq 1\,, \tag{2}$$

where Ω is the upper hemisphere.

An alternative parameterisation of the 4D directional space was proposed by Rusinkiewicz [28], in terms of the half and difference vectors $\boldsymbol{h}, \boldsymbol{d}$ or their spherical coordinates $\theta_{\boldsymbol{h}}, \phi_{\boldsymbol{h}}, \theta_{\boldsymbol{d}}, \phi_{\boldsymbol{d}}$. This coordinate system aligns the features of common BRDFs with the coordinate axes, thus providing a simpler representation with the following advantages:

- The direction of mirror reflection is fixed at $\theta_{\boldsymbol{h}} = 0$.
- Isotropic materials are independent of $\phi_{\boldsymbol{h}}$.
- Helmholtz can be expressed as a simple π-periodicity in $\phi_{\boldsymbol{d}}$:

$$f_r(\theta_{\boldsymbol{h}}, \theta_{\boldsymbol{d}}, \phi_{\boldsymbol{d}}) = f_r(\theta_{\boldsymbol{h}}, \theta_{\boldsymbol{d}}, \phi_{\boldsymbol{d}} + \pi). \tag{3}$$

Neural BRDFs (NBRDFs) [30] are proposed to model BRDF functions. A neural BRDF $f_r^{\boldsymbol{\xi}}(\theta_{\boldsymbol{h}}, \theta_{\boldsymbol{d}}, \phi_{\boldsymbol{d}})$ is a lightweight MLP network parameterised by $\boldsymbol{\xi}$ trained to overfit to a given material. However, as encoded in an MLP, two fundamental physical properties of a BRDF function, namely Helmholtz reciprocity and energy conservation, are not guaranteed. This causes undesirable effects. For example, as illustrated in Fig. 1, not adhering to Helmholtz reciprocity creates tangential discontinuities around the specular region for NBRDF models.

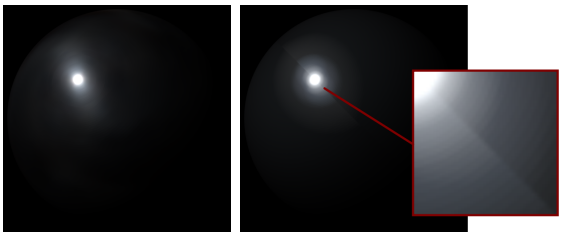

Groundtruth NBRDF [30]

Fig. 1: NBRDF [30] does not obey Helmholtz reciprocity, leading to tangential discontinuities in the specular region (see diagonal discontinuity in the close-up inset on the bottom right).

4 Method

4.1 Doubling $\phi_{\boldsymbol{d}}$ for Helmholtz Reciprocity

Helmholtz reciprocity is characterised by π-periodicity in $\phi_{\boldsymbol{d}}$, as detailed in Eq. (3). NBRDFs [30] leverage Rusinkiewicz parameterisation [28] and expect as input the spherical coordinates $\theta_{\boldsymbol{h}}, \phi_{\boldsymbol{h}}, \theta_{\boldsymbol{d}}, \phi_{\boldsymbol{d}}$ of the half and difference vectors $\boldsymbol{h}, \boldsymbol{d}$. As

$$\boldsymbol{d} = (\sin\theta_{\boldsymbol{d}} \cos\phi_{\boldsymbol{d}}, \sin\theta_{\boldsymbol{d}} \sin\phi_{\boldsymbol{d}}, \cos\theta_{\boldsymbol{d}}), \tag{4}$$

NBRDFs already exhibit 2π-periodicity in $\phi_{\boldsymbol{d}}$. To achieve the desired π-periodicity, we multiply $\phi_{\boldsymbol{d}}$ by two upon receiving it from the input. While this adjustment loses the underlying physical meaning of $\phi_{\boldsymbol{d}}$ in the network computation, it inherently ensures compliance with Helmholtz reciprocity.

4.2 Energy Amplification Loss for Energy Conservation

Non-conservation of energy (see Eq. (2)) for a BRDF can lead to noticeable artefacts. Therefore, we define an *energy amplification loss (EAL)* to measure the increment of energy for a neural BRDF $f_r^{\boldsymbol{\xi}}$:

$$\mathcal{L}_{\text{EAL}}\left(f_r^{\boldsymbol{\xi}}\right) := \int_{\Omega} h_{\text{ReLU}}\left(\int_{\Omega} f_r^{\boldsymbol{\xi}}(\boldsymbol{\omega}_i, \boldsymbol{\omega}_o)\cos\theta_o \mathrm{d}\boldsymbol{\omega}_o - 1\right)\mathrm{d}\boldsymbol{\omega}_i, \tag{5}$$

where Ω is the upper hemisphere and h_{ReLU} is the rectified linear unit [1]. During training, we add EAL to the original loss to penalise the non-conservation of energy.

4.3 Chromaticity Loss

Reflectance value fitting is sensitive to the distribution of errors, since the BRDF can have a very high dynamic range. For low values, the proportion of individual colour channels will be heavily affected by small fitting errors, leading to inaccurate tint in the rendered images. NBRDFs [30] addressed some of these issues in the fitting by using a log-loss between BRDF values:

$$\mathcal{L}_{\text{NBRDF}}(f_r^{\boldsymbol{\xi}}) := \left|\log(1 + f_r(\boldsymbol{\omega}_i, \boldsymbol{\omega}_o)\cos\theta_i) - \log(1 + f_r^{\boldsymbol{\xi}}(\boldsymbol{\omega}_i, \boldsymbol{\omega}_o)\cos\theta_i)\right|, \tag{6}$$

where f_r is the groundtruth BRDF to which $f_r^{\boldsymbol{\xi}}$ overfits. While this ensures a more balanced consideration of low-value vs high-value samples in the training, this loss is computed per-channel. It hence considers each colour individually, not addressing the disproportionate shift in tint to red that can occur at very low BRDF values if, for example, the red value is slightly overestimated while green and blue are slightly underestimated. To mitigate this inaccuracy, we introduce a *chromaticity loss (CL)*.

Directly supervising the proportion of red, green, and blue in the signal proves to be an unstable loss due to the division. Instead, we enforce some consistency between the individual channels in an indirect way by matching the norm of the predicted RGB vector with the ground truth. This encourages the error to be more consistently spread across the three channels, which in turn ensures that the NBRDF's tint is closer to the ground truth. Specifically, we formulate the chromaticity loss as the same log-weighted loss as on the individual RGB channels, except it is computed on the squared norm of the RGB vectors:

$$\mathcal{L}_{\text{CL}}(f_r^{\boldsymbol{\xi}}) := \left|\log(1 + \|f_r(\boldsymbol{\omega}_i, \boldsymbol{\omega}_o)\cos\theta_i)\|^2) - \log(1 + \left\|f_r^{\boldsymbol{\xi}}(\boldsymbol{\omega}_i, \boldsymbol{\omega}_o)\cos\theta_i)\right\|^2)\right|, \tag{7}$$

where $\|\cdot\|^2$ is the sum of squared RGB components.

5 Results and Analysis

5.1 Dataset

We leverage the MERL BRDF dataset [19] that contains reflectance functions of 100 different materials stored as densely measured BRDF values. Following [30], we overfit our PBNBRDF $f_r^{\boldsymbol{\xi}}$ to each individual material $M \in \mathcal{D}$.

5.2 Helmholtz Reciprocity

Metrics We employ two metrics to assess compliance with Helmholtz reciprocity for neural BRDFs $f_r^{\boldsymbol{\xi}}$: *Helmholtz reciprocity loss (HRL)* (Eq. (8)) and *Helmholtz continuity loss (HCL)* (Eq. (9)):

$$\mathcal{L}_{\text{HRL}}\left(f_r^{\boldsymbol{\xi}}\right) := \mathop{\mathbb{E}}_{\substack{\theta_{\boldsymbol{h}},\theta_{\boldsymbol{d}}\sim\mathcal{U}[0,\frac{\pi}{2}]\\ \phi_{\boldsymbol{d}}\sim\mathcal{U}[0,\pi]}} \left[\left(f_r^{\boldsymbol{\xi}}(\theta_{\boldsymbol{h}},\theta_{\boldsymbol{d}},\phi_{\boldsymbol{d}}) - f_r^{\boldsymbol{\xi}}(\theta_{\boldsymbol{h}},\theta_{\boldsymbol{d}},\phi_{\boldsymbol{d}}+\pi)\right)^2\right]; \tag{8}$$

$$\mathcal{L}_{\text{HCL}}\left(f_r^{\boldsymbol{\xi}}\right) := \mathop{\mathbb{E}}_{\theta_{\boldsymbol{h}},\theta_{\boldsymbol{d}}\sim\mathcal{U}[0,\frac{\pi}{2}]} \left[\left|f_r^{\boldsymbol{\xi}}(\theta_{\boldsymbol{h}},\theta_{\boldsymbol{d}},0) - f_r^{\boldsymbol{\xi}}(\theta_{\boldsymbol{h}},\theta_{\boldsymbol{d}},\pi)\right|\right], \tag{9}$$

where $\mathcal{U}[a,b]$ is the uniform distribution on the interval $[a,b]$. HRL quantifies the degree of enforcement of Helmholtz across the entire domain of $\phi_{\boldsymbol{d}} \in [0,2\pi]$. Nevertheless, the domain boundaries are of particular significance since any disparity between $f_M(\theta_{\boldsymbol{h}},\theta_{\boldsymbol{d}},\phi_{\boldsymbol{d}}=0)$ and $f_M(\theta_{\boldsymbol{h}},\theta_{\boldsymbol{d}},\phi_{\boldsymbol{d}}=\pi)$ for given $\theta_{\boldsymbol{h}},\theta_{\boldsymbol{d}}$ values might manifest as a pronounced discontinuity in the rendered images, even if the difference is minimal. To address this, we introduce HCL as an additional metric to quantify such discontinuities in rendering. Both metrics aim for lower values to indicate better performance.

We present our quantitative results in Tab. 1 and qualitative results in Fig. 2. In Tab. 1 the negligible HRL and HCL values for PBNBRDF indicate its strong adherence to Helmholtz reciprocity. From Fig. 2 we can observe that violating Helmholtz reciprocity creates tangential discontinuities in NBRDF renderings. In contrast, our PBNBRDF gives more natural and high-quality renderings without noticeable discontinuity.

Model	HRL$\times 10^3(\downarrow)$	HCL$\times 10^3(\downarrow)$
Groundtruth	0	0
NBRDF [30]	14729	52
PBNBRDF (ours)	**43**	**2**

Table 1: Comparison of adherence to Helmholtz reciprocity. The vanishing HRL and HCL for PBNBRDF indicate its strong adherence to Helmholtz reciprocity.

5.3 Energy Conservation

Metrics We use mean absolute error (MAE), peak signal-to-noise ratio (PSNR), and structural similarity index measure (SSIM) to evaluate the rendered images. The metrics are computed on the images rendered from the ground-truth (MERL BRDF [19]) and from the neural models. MAE aims for lower values for better performance whereas PSNR and SSIM aim for the higher.

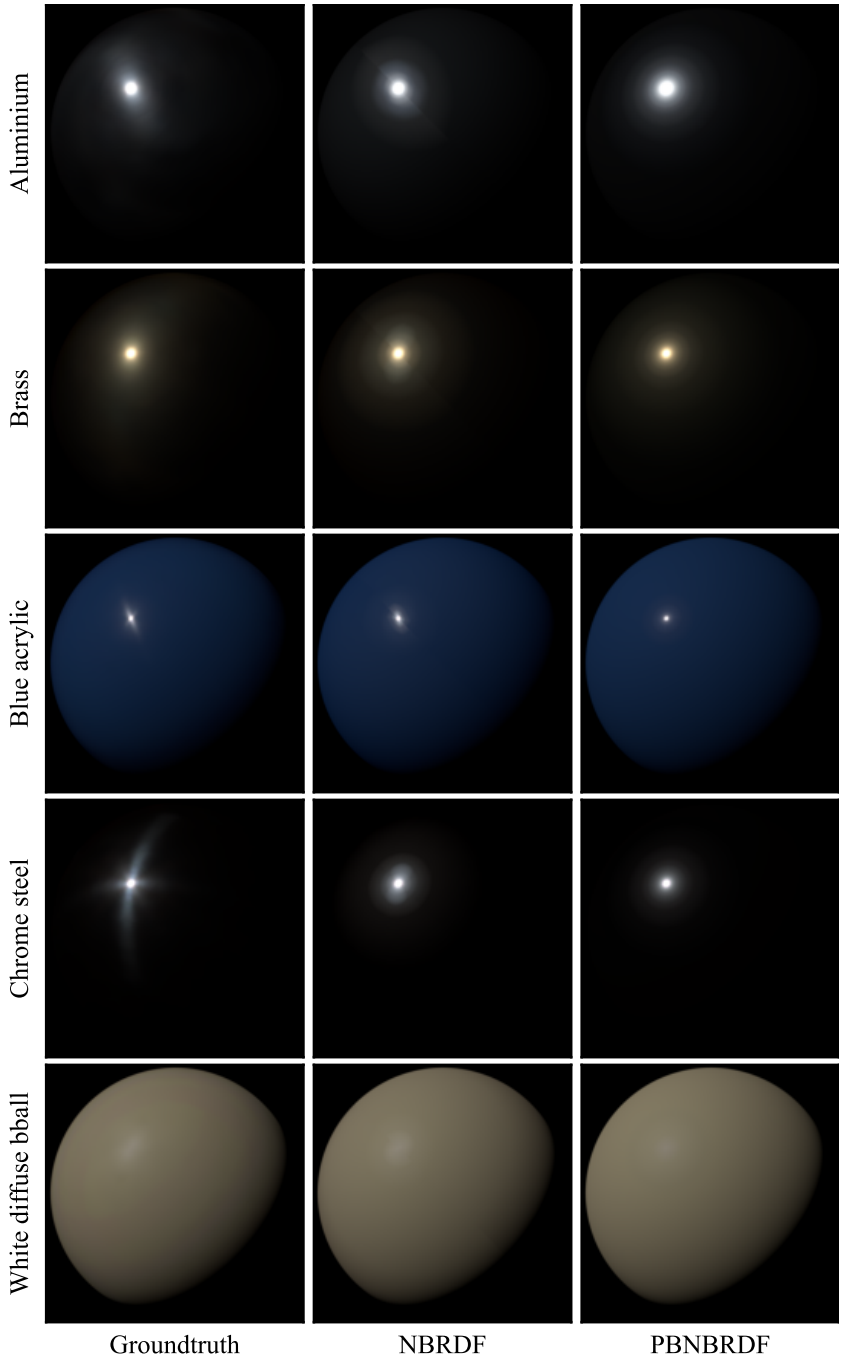

Fig. 2: Renderings of neural models. Note that violating Helmholtz reciprocity creates tangential discontinuities in NBRDF renderings, whereas our PBNBRDF gives more natural and high-quality renderings without noticeable discontinuity.

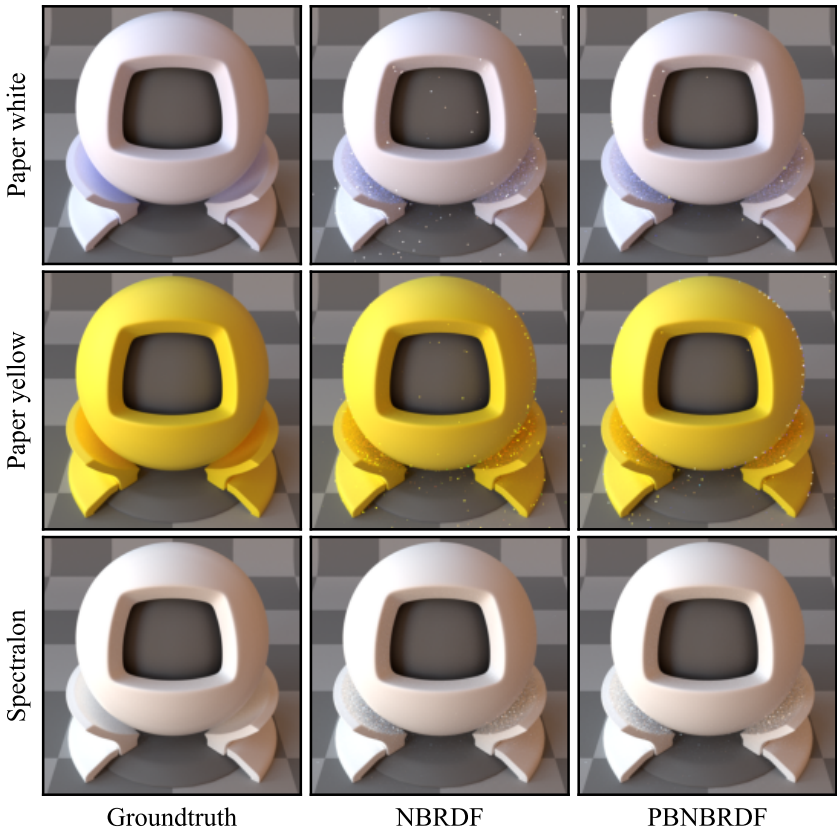

Fig. 3: Renderings of neural models evaluated on materials from the Realistic Graphics Lab (RGL) database [7], characterised by very low energy dissipation. Note that the fitting of these materials with NBRDF results in noticeable artifacts (fireflies) due to energy amplification. The effect is reduced when using our PBNBRDF.

Model	MAE$\times 10^3$(↓)	PSNR(↑)	SSIM(↑)
NBRDF [30]	6.42	47.4	**0.978**
PBNBRDF (ours)	**6.10**	**47.8**	**0.978**

Table 2: EAL (Eq. (5)) facilitates the energy conservation, leading to an improvement of image quality metrics.

In Fig. 3 we display renderings of a selection of materials from the Realistic Graphics Lab (RGL) database [7]. This set corresponds to the BRDFs with the lowest dissipation of energy, such as *spectralon*. When fitted using NBRDF, the unconstrained regression of these materials leads to artefacts due to non-conservation of energy. Our unsupervised energy loss EAL (Eq. (5)) reduces this effect by penalising energy amplification, leading to an improvement of image quality metrics, as demonstrated in Tab. 2.

5.4 Chromaticity Regularisation

Metrics We use five evaluation metrics: mean absolute error (MAE), mean squared error (MSE), learned perceptual image patch similarity (LPIPS) [37], peak signal-to-noise ratio (PSNR), and structural similarity index measure (SSIM). The first three metrics aim for lower values for better performance whereas the last two aim for the higher.

Model	MAE(↓)	MSE(↓)	LPIPS$\times 10^3$(↓)	PSNR(↑)	SSIM(↑)
NBRDF [30]	0.805	2.45	9.11	32.9	0.988
PBNBRDF (ours)	**0.586**	**1.31**	**6.76**	**36.8**	**0.992**

Table 3: Comparison of the two models rendered images. PBNBRDF consistently achieve superior performance across all metrics, indicating the effectiveness of the chromaticity regularisation.

In Tab. 3, we conduct a comparative evaluation of images rendered using the original NBRDF method [30] and our proposed PBNBRDF method. The results clearly demonstrate that images produced by the PBNBRDF method exhibit consistently higher performance across all evaluated metrics. This enhancement underscores the efficacy of chromaticity regularisation within the PBNBRDF framework.

6 Conclusion

Neural Fields have proven their efficiency in modelling material appearance, through their expressiveness and compactness of representation coupled with high fidelity to the real-world training data. However, these neural functions are completely unconstrained, which might lead to important artifacts in physical simulations like path tracing, where BRDFs are expected to satisfy strict physical constraints. We show that enforcing respect of these properties, either through losses during training, or through network design choices, not only produces more stable Neural BRDFs, but even preserves more fidelity to the ground truth, which highlights the importance of informing neural network architectures and training with physical laws.

References

1. Agarap, A.F.: Deep learning using rectified linear units (relu). arXiv preprint arXiv:1803.08375 (2018) 5
2. Bangay, S., Radloff, J.D.: Kaleidoscope configurations for reflectance measurement. In: Proceedings of the 3rd International Conference on Computer Graphics, Virtual Reality, Visualisation and Interaction in Africa. p. 161–170. AFRIGRAPH '04, Association for Computing Machinery, New York, NY, USA (2004). https://doi.org/10.1145/1029949.1029979, https://doi.org/10.1145/1029949.1029979 2
3. Burley, B.: Physically-based shading at disney. SIGGRAPH Comput. Graph. (2012), https://api.semanticscholar.org/CorpusID:7260137 2
4. Cook, R.L., Torrance, K.E.: A reflectance model for computer graphics. ACM Trans. Graph. **1**(1), 7–24 (jan 1982). https://doi.org/10.1145/357290.357293, https://doi.org/10.1145/357290.357293 2
5. Dana, K.J., van Ginneken, B., Nayar, S.K., Koenderink, J.J.: Reflectance and texture of real-world surfaces. ACM Trans. Graph. **18**(1), 1–34 (jan 1999). https://doi.org/10.1145/300776.300778, https://doi.org/10.1145/300776.300778 2
6. Dou, Y., Zheng, Z., Jin, Q., Ni, B., Chen, Y., Ke, J.: Real-time neural BRDF with spherically distributed primitives. CoRR **abs/2310.08332** (2023). https://doi.org/10.48550/ARXIV.2310.08332, https://doi.org/10.48550/arXiv.2310.08332 3
7. Dupuy, J., Jakob, W.: An adaptive parameterization for efficient material acquisition and rendering. Transactions on Graphics (Proceedings of SIGGRAPH Asia) **37**(6), 274:1–274:18 (Nov 2018). https://doi.org/10.1145/3272127.3275059 2, 8, 9
8. Fan, J., Wang, B., Hašan, M., Yang, J., Yan, L.Q.: Neural layered brdfs. In: Proceedings of SIGGRAPH 2022 (2022) 3
9. Fischer, M., Ritschel, T.: Metappearance: Meta-learning for visual appearance reproduction. ACM Trans Graph (Proc. SIGGRAPH Asia) **41**(4) (2022) 3
10. Guarnera, D., Guarnera, G., Ghosh, A., Denk, C., Glencross, M.: Brdf representation and acquisition. Computer Graphics Forum **35**(2), 625–650 (2016). https://doi.org/https://doi.org/10.1111/cgf.12867, https://onlinelibrary.wiley.com/doi/abs/10.1111/cgf.12867 2
11. Guarnera, D., Guarnera, G.C., Ghosh, A., Denk, C., Glencross, M.: BRDF Representation and Acquisition. Computer Graphics Forum (2016). https://doi.org/10.1111/cgf.12867 1
12. Guo, J., Li, Z., He, X., Wang, B., Li, W., Guo, Y., Yan, L.Q.: Metalayer: A meta-learned bsdf model for layered materials. ACM Trans. Graph. **42**(6) (dec 2023). https://doi.org/10.1145/3618365, https://doi.org/10.1145/3618365 3
13. Hu, B., Guo, J., Chen, Y., Li, M., Guo, Y.: Deepbrdf: A deep representation for manipulating measured brdf. Computer Graphics Forum **39**(2), 157–166 (2020). https://doi.org/https://doi.org/10.1111/cgf.13920, https://onlinelibrary.wiley.com/doi/abs/10.1111/cgf.13920 3
14. Lafortune, E.P.F., Foo, S.C., Torrance, K.E., Greenberg, D.P.: Non-linear approximation of reflectance functions. In: Proceedings of the 24th Annual Conference on Computer Graphics and Interactive Techniques. p. 117–126. SIGGRAPH '97, ACM Press/Addison-Wesley Publishing Co., USA (1997). https://doi.org/10.1145/258734.258801, https://doi.org/10.1145/258734.258801 2

15. Lawrence, J., Rusinkiewicz, S., Ramamoorthi, R.: Efficient brdf importance sampling using a factored representation. In: ACM SIGGRAPH 2004 Papers. p. 496–505. SIGGRAPH '04, Association for Computing Machinery, New York, NY, USA (2004). https://doi.org/10.1145/1186562.1015751, https://doi.org/10.1145/1186562.1015751 2
16. Li, H., Foo, S.C., Torrance, K.E., Westin, S.H.: Automated three-axis gonioreflectometer for computer graphics applications. Optical Engineering **45**(4), 043605 (2006). https://doi.org/10.1117/1.2192787, https://doi.org/10.1117/1.2192787 2
17. Liu, C., Fischer, M., Ritschel, T.: Learning to learn and sample brdfs. Computer Graphics Forum (Proceedings of Eurographics) **42**(2), 201–211 (2023). https://doi.org/10.1111/cgf.14754 3
18. Marschner, S.R., Westin, S.H., Lafortune, E.P.F., Torrance, K.E., Greenberg, D.P.: Image-Based BRDF Measurement Including Human Skin. In: Lischinski, D., Larson, G.W. (eds.) Eurographics Workshop on Rendering. The Eurographics Association (1999). https://doi.org/10.2312/EGWR/EGWR99/131-144 2
19. Matusik, W., Pfister, H., Brand, M., McMillan, L.: A data-driven reflectance model. ACM Transactions on Graphics (TOG) **22**(3), 759–769 (Jul 2003). https://doi.org/10.1145/882262.882343, https://www.merl.com/publications/TR2003-832, 5, 6
20. Mildenhall, B., Srinivasan, P.P., Tancik, M., Barron, J.T., Ramamoorthi, R., Ng, R.: Nerf: Representing scenes as neural radiance fields for view synthesis. In: ECCV (2020) 1
21. Ngan, A., Durand, F., Matusik, W.: Experimental Analysis of BRDF Models. In: Bala, K., Dutre, P. (eds.) Eurographics Symposium on Rendering (2005). The Eurographics Association (2005). https://doi.org/10.2312/EGWR/EGSR05/117-126 2
22. Nicodemus, F.E., Richmond, J.C., Hsia, J.J., Ginsberg, I.W., Limperis, T.: Geometrical considerations and nomenclature for reflection. Tech. Rep. 160, National Bureau of Standards (1977) 3
23. Nicodemus, F.E., Richmond, J.C., Hsia, J.J., Ginsberg, I.W., Limperis, T., Harman, S., Baruch, J.J.: Geometrical considerations and nomenclature for reflectance (1977), https://api.semanticscholar.org/CorpusID:18645782 1
24. Nielsen, J.B., Jensen, H.W., Ramamoorthi, R.: On optimal, minimal brdf sampling for reflectance acquisition. ACM Trans. Graph. **34**(6) (nov 2015). https://doi.org/10.1145/2816795.2818085, https://doi.org/10.1145/2816795.2818085 2
25. Phong, B.T.: Illumination for computer generated pictures. Commun. ACM **18**(6), 311–317 (jun 1975). https://doi.org/10.1145/360825.360839, https://doi.org/10.1145/360825.360839 2
26. Rainer, G., Bousseau, A., Ritschel, T., Drettakis, G.: Neural precomputed radiance transfer. Computer Graphics Forum (Proceedings of the Eurographics conference) **41**(2) (April 2022), http://www-sop.inria.fr/reves/Basilic/2022/RBRD22 1
27. Rainer, G., Jakob, W., Ghosh, A., Weyrich, T.: Neural BTF compression and interpolation. Computer Graphics Forum (Proc. Eurographics) **38**(2), 235–244 (May 2019) 1
28. Rusinkiewicz, S.: A new change of variables for efficient BRDF representation. Vienna, Austria (Jun 1998) 4
29. Sitzmann, V., Martel, J.N., Bergman, A.W., Lindell, D.B., Wetzstein, G.: Implicit neural representations with periodic activation functions. In: Proc. NeurIPS (2020) 1

30. Sztrajman, A., Rainer, G., Ritschel, T., Weyrich, T.: Neural brdf representation and importance sampling. Computer Graphics Forum (2021). https://doi.org/https://doi.org/10.1111/cgf.14335, https://onlinelibrary.wiley.com/doi/abs/10.1111/cgf.14335 1, 3, 4, 5, 6, 8, 9
31. Walter, B., Marschner, S.R., Li, H., Torrance, K.E.: Microfacet models for refraction through rough surfaces. In: Proceedings of the 18th Eurographics Conference on Rendering Techniques. p. 195–206. EGSR'07, Eurographics Association, Goslar, DEU (2007) 2
32. Wang, P., Liu, L., Liu, Y., Theobalt, C., Komura, T., Wang, W.: Neus: Learning neural implicit surfaces by volume rendering for multi-view reconstruction. NeurIPS (2021) 1
33. Ward, G.J.: Measuring and modeling anisotropic reflection. SIGGRAPH Comput. Graph. **26**(2), 265–272 (jul 1992). https://doi.org/10.1145/142920.134078, https://doi.org/10.1145/142920.134078 2
34. Weinmann, M., Gall, J., Klein, R.: Material Classification Based on Training Data Synthesized Using a BTF Database. In: Computer Vision - ECCV 2014 - 13th European Conference, Zurich, Switzerland, September 6-12, 2014, Proceedings, Part III. pp. 156–171. Springer International Publishing (2014) 2
35. White, D.R., Saunders, P., Bonsey, S.J., van de Ven, J., Edgar, H.: Reflectometer for measuring the bidirectional reflectance of rough surfaces. Appl. Opt. **37**(16), 3450–3454 (Jun 1998). https://doi.org/10.1364/AO.37.003450, https://opg.optica.org/ao/abstract.cfm?URI=ao-37-16-3450 2
36. Zeltner, T., Rousselle, F., Weidlich, A., Clarberg, P., Novák, J., Bitterli, B., Evans, A., Davidovič, T., Kallweit, S., Lefohn, A.: Real-time neural appearance models. arXiv preprint arXiv:2305.02678 (2023) 3
37. Zhang, R., Isola, P., Efros, A.A., Shechtman, E., Wang, O.: The unreasonable effectiveness of deep features as a perceptual metric. In: CVPR (2018) 9
38. Zheng, C., Zheng, R., Wang, R., Zhao, S., Bao, H.: A compact representation of measured brdfs using neural processes. ACM Trans. Graph. **41**(2) (nov 2021). https://doi.org/10.1145/3490385, https://doi.org/10.1145/3490385 3